

A natural NISQ model of quantum self-attention mechanism

Shangshang Shi ^a, Zhimin Wang ^{a,*}, Jiaxin Li ^a, Yanan Li ^a, Ruimin Shang ^a, Haiyong Zheng ^a, Guoqiang Zhong ^a, and Yongjian Gu ^a

^a Faculty of Information Science and Engineering, Ocean University of China, Qingdao, China

*Corresponding author: Zhimin Wang, wangzhimin@ouc.edu.cn

Abstract

The self-attention mechanism (SAM) has demonstrated remarkable success in various applications. However, training SAM on classical computers becomes computationally challenging as the number of trainable parameters grows. Quantum neural networks (QNNs) have been developed as a novel learning model that promises to provide speedup for pattern recognition using near-term Noisy Intermediate-Scale Quantum (NISQ) computers. In this work, we propose a completely natural way of implementing SAM in QNNs, resulting in the quantum self-attention mechanism (QSAM). The fundamental operations of SAM, such as calculating attention scores and producing attention features, are realized by only designing the data encoding and ansatz architecture appropriately. As these are the fundamental components of QNNs, our QSAM can be executed efficiently on near-term NISQ devices. Our QSAM models achieve better performance in terms of both accuracy and circuit complexity on the text categorization task. Moreover, the robustness of QSAM against various typical types of quantum noise is demonstrated, indicating the model's suitability for NISQ devices. The present QSAM will serve as the fundamental building blocks for developing large models of quantum attention neural networks for quantum advantageous applications.

Keywords: Quantum neural networks, Quantum self-attention mechanism, Noisy intermediate-scale quantum computer, Text categorization

1. Introduction

The self-attention mechanism (SAM) is a critical component of many powerful deep learning architectures that have achieved state-of-the-art performance across various tasks such as natural language processing [1-2] and computer vision [3-4]. Unlike convolutional and recurrent models, which process only one local neighborhood at a time, SAM is based on non-local operations [4], allowing it to capture long-range dependencies within the features and understand the data from a global perspective. This unique advantage has contributed to the excellent performance of SAM-based architectures [5]. However, SAM's quadratic complexity makes it

computationally inefficient, severely limiting its applicability, especially when equipped with up to hundreds of billions of parameters, making it extremely challenging to train on classical computing resources [6].

In recent years, remarkable breakthroughs have been made in the field of quantum computing [7-9]. Notably, people are now entering the NISQ era of quantum computing, where NISQ refers to noisy intermediate-scale quantum computing [10]. There is a growing consensus that near-term NISQ devices will have advantageous applications by exploiting NISQ algorithms [11]. One of the most promising approaches is the development of quantum neural networks (QNNs) [12-13]. As a quantum analogue of

classical neural networks, QNNs leverage parameterized quantum circuits (PQC) as a learning model [14], and can extend to deep neural networks with flexible multilayer architectures, such as quantum convolutional neural networks (QCNNs) [15-16] and quantum recurrent neural networks (QRNNs) [17-18].

QRNNs have the potential for more powerful learnability by utilizing the exponential large feature space generated by the PQC. To fully explore this huge space and capture long-range dependencies within the features, the SAM is necessary for QRNNs. However, currently there is no natural approach to implementing SAM in QNNs, where “natural” means that the mechanism should be integrated into the fundamental architecture of PQC. For reference, Cong et al. [15] proposed a natural NISQ model of QCNN that implements the convolutional and pooling mechanisms by appropriately designing the PQC. Developing a similar natural model of quantum self-attention mechanism (QSAM) is necessary for the advancement of QNNs.

So far, the following QSAM models have been proposed. Zhao et al. [19] introduced the quantum logical similarity (QLS) technique to evaluate attention scores and constructed a quantum self-attention neural network. While capable of efficiently computing attention scores, this model has a high circuit complexity, requiring several large auxiliary quantum registers and swap operations between registers. Li et al. [20] developed a quantum-classical hybrid self-attention neural network, where quantum circuits are mainly used to prepare *Query*, *Key*, and *Value* representations in the high-dimensional quantum feature space, while attention score calculations and weighted summation are implemented on the classical computer. A similar idea was also used by Sipio et al. [21] to construct a quantum Transformer. Such hybrid

models only take quantum circuits as performance-enhanced versions of feedforward neural networks to replace those in the original classical models, and face interface problems between quantum and classical systems.

In this paper, we propose a natural and completely NISQ-compliant model of QSAM. Our main idea is based on the following fundamental observations: (1) the most basic operation in QNNs is implementing a PQC, which has adjustable quantum gates and can be trained to approximate almost any target function; (2) the key operations of SAM involve calculating attention scores and producing new features based on those scores. We find that the SAM operations can be naturally realized by properly designing the way of data encoding and the architecture of PQC. As a result, our QSAM is much more accessible on near-term NISQ devices.

The main contributions of this work are as follows:

(1) We develop a novel approach for implementing SAM in QNNs by combining the way of data encoding and PQC architecture. Our model is natural in terms of QNNs, because all the components required in this model are the properly-designed data encoding circuit and PQC which are most basic components of QNNs.

(2) The entire quantum circuit of our QSAM is hardware efficient, and can be customized concerning the gate set and connectivity of the quantum devices on hand. As a result, our QSAM can be executed efficiently on a variety of NISQ systems.

(3) Our QSAM achieves better performance compared to other quantum learning models on the task of text categorization using public datasets. In addition, our model is robust against various typical types of quantum noise, demonstrating its suitability for near-term NISQ devices.

The rest of the paper is organized as

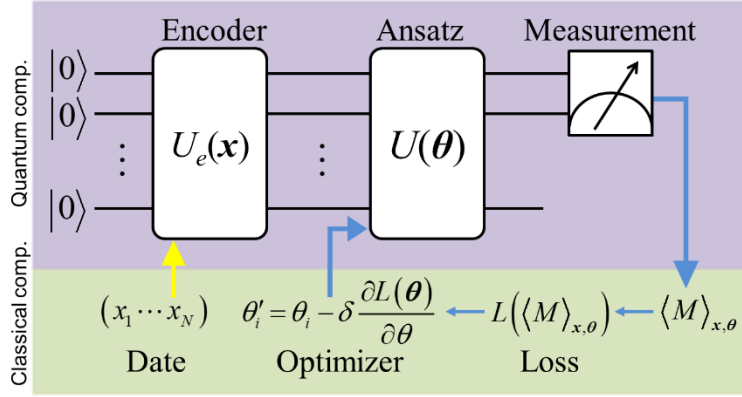


Fig. 1. The architecture of QNN. QNN is a hybrid machine learning model that combines quantum and classical computing, where the forward feature map is implemented on the quantum computer and parameter optimization is done on the classical computer.

follows. Section 2 reviews preliminary concepts about QNNs and SAM that will be used in this paper. Section 3 discusses the details of our QSAM architecture. Section 4 presents experimental results of QSAM’s performance on tasks such as Iris flower classification and text categorization, as well as its robustness against quantum noise. Finally, we conclude our work in Section 5.

2. Preliminaries

2.1. Quantum neural networks

QNNs are quantum analogue of classical neural networks, which use PQC as machine learning models [22]. Generally, QNN consists of four parts: data encoder, ansatz, quantum measurement and parameter optimization routine, as shown in Fig. 1. The first three parts are implemented on the quantum computer, while the last optimization routine is carried out on the classical computer.

The encoder circuit is used to represent classical data as quantum states, which involves performing the unitary transformation $|\mathbf{x}\rangle = U_e |0\rangle^{\otimes n}$, where \mathbf{x} is the data vector. Data encoding can be seen as a quantum feature map, which maps the data space to the Hilbert space where quantum states exist [23]. One of the commonly used encoding method is angle encoding that embeds

data into the rotation angles of single-qubit or two-qubit rotation gates [24]. In the experiments of this paper, we use this method.

Ansatz circuit is a quantum analogue of classical feedforward neural network and is utilized to identify patterns within the feature generated by the encoder circuit. Ansatz is in fact a PQC consisting of adjustable quantum gates. Parameters in ansatz are optimized to approximate the target function that maps the feature to different value domains, each representing a distinct class.

There are generally two approaches to designing ansatz circuit, i.e. problem-inspired and hardware-efficient methods [22, 25-27]. The problem-inspired method requires the Hamiltonian related to the problem to construct the circuit, while the hardware-efficient method is directly assembling the native single-qubit and two-qubit gates based on the gate set and connectivity of the available quantum devices [27]. Therefore, hardware-efficient ansatz can be implemented efficiently on near-term NISQ devices.

Quantum measurement is utilized to generate a prediction or label for the inputting data [28]. The measurement corresponds to a physical observable M , that can be decomposed as

$M = \sum_i \lambda_i |\lambda_i\rangle\langle\lambda_i|$, where λ_i is the i^{th} eigenvalue and $|\lambda_i\rangle$ is the corresponding eigenstate. After a measurement M , the quantum state $|\varphi\rangle$ will collapse to one of the eigenstates $|\lambda_i\rangle$ with the probability $p_i = |\langle\lambda_i|\varphi\rangle|^2$, and the expectation of measurement outcome can be expressed as

$$\langle M \rangle = \sum_i \lambda_i \cdot p_i = \sum_i \lambda_i |\langle\lambda_i|\varphi\rangle|^2. \quad (1)$$

The most frequently employed measurement in quantum algorithms is the computational basis measurement, namely the Pauli-Z measurement as follows:

$$\sigma_z = (+1)|0\rangle\langle 0| + (-1)|1\rangle\langle 1|. \quad (2)$$

Optimization routine is used to update ansatz circuit's parameters, i.e. the rotation angles of gates. Much like classical models, the optimization process involves defining a loss function $L(\theta)$ and minimizing it in terms of the parameter vector θ . In QNN, commonly used loss functions such as mean squared error and cross-entropy loss can be utilized.

Similar to classical neural networks, parameters of ansatz can be updated using the gradient of the loss function. For instance, in the gradient descent method, we can update the i^{th} parameter θ_i as follows:

$$\theta'_i = \theta_i - \delta \cdot \partial L(\theta) / \partial \theta_i, \quad (3)$$

where δ is known as the learning rate. It's worth noting that QNNs have no the backpropagation algorithm for evaluating gradient of parameters. Instead, the gradient is computed using techniques such as difference method or parameter shift rule on quantum computers [29-30].

2.2. Self-attention mechanism

SAM is a variant of attention mechanism that computes a representation of a sequence or image by

relating different positions within it. In SAM, attention is calculated entirely based on feature vectors of the input data. Specifically, given a data sample (x_1, \dots, x_N) with $x_i \in \mathbb{R}^d$, first three sets of feature vectors called *Query*, *Key* and *Value* are computed as

$$Q_i = W_Q \cdot x_i, \quad K_i = W_K \cdot x_i, \quad V_i = W_V \cdot x_i, \quad (4)$$

where $W_Q, W_K, W_V \in \mathbb{R}^{d \times d}$ represent the parameter matrices required to learn.

Then, the relevance of each *Key* position to the *Query* position is evaluated using a compatibility function. The resulting relevance score, namely attention score, represents the similarity or compatibility between the two positions, indicating how relevant a particular *Key* position is to the *Query* position. The two commonly used compatibility functions are additive function and dot-product function [31]. The dot-product function computes the attention scores as follows:

$$a_{ij} = Q_i \cdot K_j^T, \quad (5)$$

and the additive function uses the following way

$$a_{ij} = f(Q_i, K_j), \quad (6)$$

where $f(\cdot)$ is implemented using a feedforward neural network.

Finally, the attention at position i is computed through a weighted sum of *Value* vector at all positions. Specifically,

$$attent_i = \sum_{j=1}^N \text{softmax}(a_{ij}) \cdot V_j, \quad (7)$$

where the softmax function is used to normalize the N attention scores. In practice, dot-product attention is faster and more space-efficient than additive attention because it can be implemented using highly optimized matrix multiplication code. The dot-product attention can be expressed in matrix form as [1],

$$attent(Q, K, V) = \text{softmax}\left(\frac{QK^T}{\sqrt{d}}\right)V, \quad (8)$$

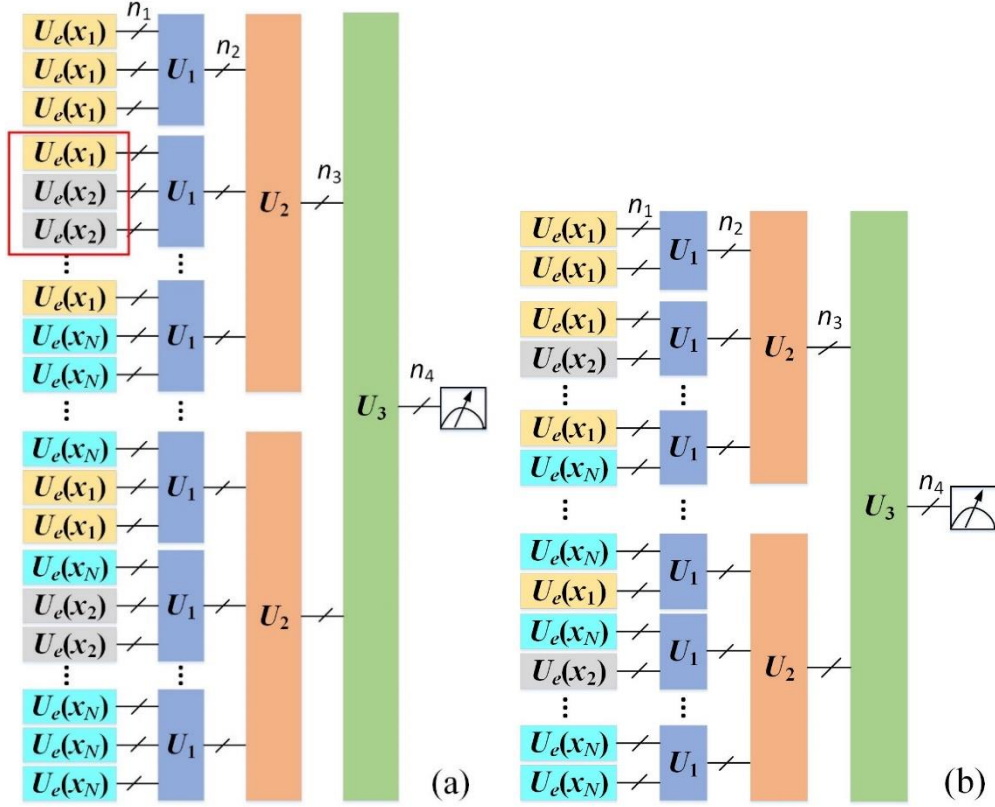


Fig. 2. Two architectures of QSAM, (a) the basic architecture (named QSAMb) and (b) the optimized version (named QSAMo). U_e represents the encoding circuit, and U_1 , U_2 and U_3 are the ansatz used to approximate target functions.

where Q , K and V are matrices that contain the *Query*, *Key* and *Value* vectors, respectively, and \sqrt{d} is a scaling factor used to reduce the magnitude of dot products.

3. Quantum self-attention mechanism and associated networks

In quantum computing, the similarity between two quantum states can be characterized mathematically by their inner-product, which is typically evaluated using the SWAP test [32] or QLS method [33]. However, the resulting quantum circuits have high complexity to run on the near-term NISQ devices.

In this paper, we find that the attention vectors in the QSAM can be evaluated by properly design the way of data encoding and the architecture of PQC based on the basic spirit of classical

SAM. Specifically, Eqs. (5), (6) and (7) can be generally formalized as

$$attent_i = \sum_{j=1}^N g(Q_i, K_j) \cdot V_j, \quad (9)$$

where $g(\cdot)$ represents the dot product operation in Eq.(5) or feedforward transformation in Eq. (6). In QNN, we can put the vectors, Q_i , K_j and V_j together during the process of data encoding, and approximate the transformation $g(\cdot)$ and arithmetic operations through a PQC. Accordingly, the quantum circuit of our QSAM is designed as shown in Fig. 2, where Fig. 2(a) is the basic architecture denoted as QSAMb, and Fig. 2(b) is the optimized one denoted as QSAMo, which removes some redundant information from the QSAMb model. For example, in the encoding unit marked by the red box in Fig. 2(a), the data vector x_2 is embedded twice. In

$$\begin{bmatrix} \mathbf{att}_1 \\ \mathbf{att}_2 \\ \vdots \\ \mathbf{att}_N \end{bmatrix} = \begin{bmatrix} \mathbf{Q}_1 \\ \mathbf{Q}_2 \\ \vdots \\ \mathbf{Q}_N \end{bmatrix} \begin{bmatrix} \mathbf{K}_1^T & \mathbf{K}_2^T & \cdots & \mathbf{K}_N^T \end{bmatrix} \begin{bmatrix} \mathbf{V}_1 \\ \mathbf{V}_2 \\ \vdots \\ \mathbf{V}_N \end{bmatrix} = \begin{bmatrix} \mathbf{Q}_1 \mathbf{K}_1^T \mathbf{V}_1 + \mathbf{Q}_1 \mathbf{K}_2^T \mathbf{V}_2 + \cdots + \mathbf{Q}_1 \mathbf{K}_N^T \mathbf{V}_N \\ \mathbf{Q}_2 \mathbf{K}_1^T \mathbf{V}_1 + \mathbf{Q}_2 \mathbf{K}_2^T \mathbf{V}_2 + \cdots + \mathbf{Q}_2 \mathbf{K}_N^T \mathbf{V}_N \\ \vdots \\ \mathbf{Q}_N \mathbf{K}_1^T \mathbf{V}_1 + \mathbf{Q}_N \mathbf{K}_2^T \mathbf{V}_2 + \cdots + \mathbf{Q}_N \mathbf{K}_N^T \mathbf{V}_N \end{bmatrix}. \quad (10)$$

order to reduce the circuit complexity of the model, one of the repeated encoding circuits could be left out, which can greatly decrease the number of qubits and trainable parameters. Below, we'll illustrate the model architecture in detail using the QSAMb.

As shown in Fig. 2(a), QSAMb begins with encoding circuits, i.e. $U_e(x_i)$. The encoding circuits serve two purposes. The first purpose is to obtain the *Query*, *Key* and *Value* vectors by embedding the classical data in the quantum feature space spanned by the encoding circuits. The second one is to put the \mathbf{Q}_i , \mathbf{K}_j and \mathbf{V}_j vectors together in a manner as shown in Eq. (9). This is achieved using an encoding unit as shown by the red box in Fig. 2(a), where three encoding circuits constitute one encoding unit. It's worth noting that the quantum gates of encoding circuit can be fixed or adjustable (namely with or without trainable parameters) depending on the learning task.

The following U_1 and U_2 ansatz are used to implement the transformation $g(\cdot)$ and arithmetic operations in Eq. (9). When the $g(\cdot)$ is the dot product operation, given a data sample $(\mathbf{x}_1, \dots, \mathbf{x}_N)$, Eq. (8) can be expressed as Eq.(10). Note that the first element of the attention vector \mathbf{att}_1 equals to $\mathbf{Q}_1 \mathbf{K}_1^T \mathbf{V}_1 + \mathbf{Q}_1 \mathbf{K}_2^T \mathbf{V}_2 + \cdots + \mathbf{Q}_1 \mathbf{K}_N^T \mathbf{V}_N$. Therefore, the U_1 circuit following the red box unit in Fig. 2(a) can be regarded as performing the operation $\mathbf{Q}_1 \mathbf{K}_2^T \mathbf{V}_2$. The first N U_1 circuits output the N weighted value vectors, i.e. $\mathbf{Q}_1 \mathbf{K}_1^T \mathbf{V}_1, \mathbf{Q}_1 \mathbf{K}_2^T \mathbf{V}_2, \dots, \mathbf{Q}_1 \mathbf{K}_N^T \mathbf{V}_N$. Then the following U_2 circuit is used to approximate the operation

$\mathbf{Q}_1 \mathbf{K}_1^T \mathbf{V}_1 + \mathbf{Q}_1 \mathbf{K}_2^T \mathbf{V}_2 + \cdots + \mathbf{Q}_1 \mathbf{K}_N^T \mathbf{V}_N$ and obtain the first attention vector \mathbf{att}_1 .

When the $g(\cdot)$ is the feedforward transformation, the functionality of U_1 and U_2 circuits can also be interpreted in terms of additive compatibility function. Specifically, the U_1 circuits correspond to the feedforward neural network to obtain the attention scores as shown in Eq. (6). By harnessing the strong correlation properties of the quantum circuits (both encoding and U_1 circuits), the feature vectors, not only the attention scores are obtained, i.e. $\mathbf{a}_{ij} \tilde{\mathbf{V}}_j = f_{U_1}(\mathbf{Q}_i, \mathbf{K}_j, \tilde{\mathbf{V}}_j)$. Then the U_2 circuit is used to obtain the attention, i.e. $\mathbf{att}_i = \sum_j \mathbf{a}_{ij} \tilde{\mathbf{V}}_j$.

The final layer of our QSAM model is made up of the U_3 circuit, which is used to transform the attention vectors. It is worth noting that the attention vectors can serve as input features for the U_3 circuit, and therefore, the design of the U_3 circuit can vary depending on the nature of the input feature. For instance, it can be designed using convolutional and recurrent architectures for image and sequential data, respectively. In the end, quantum measurement is applied to output a prediction for the classification or regression task.

Here we remark that all the data encoding circuits as well as the U_1 , U_2 and U_3 circuits are implemented using the PQC. For the encoding circuits, PQCs with different structure would be adopted according to the properties of the learning data; whereas, U_1 , U_2 and U_3 could be implemented using the PQCs with the same structure. The specific structure of the PQC is discussed in the section of numerical experiments.

4. Numerical experiments

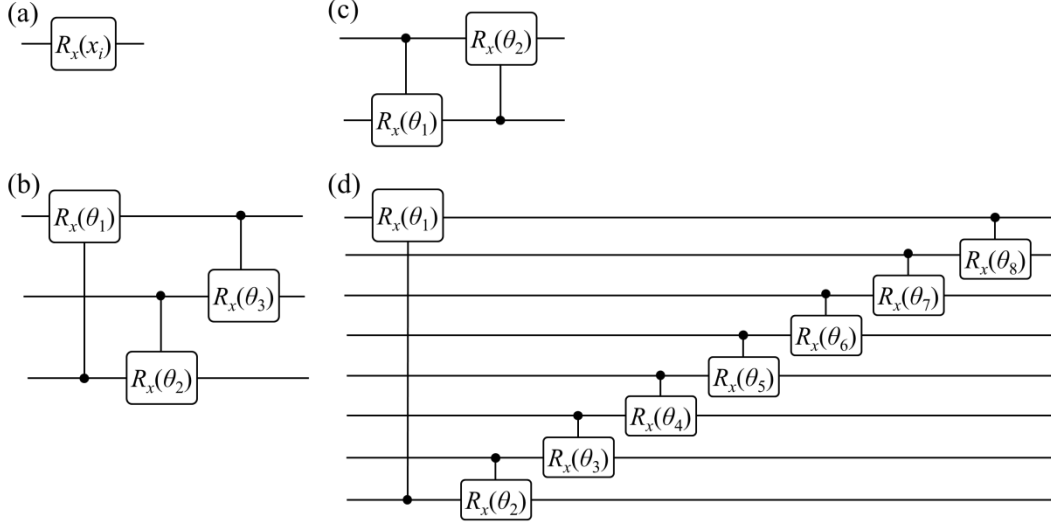


Fig. 3. The architecture of the quantum circuit for (a) data encoding unit $U_e(x_i)$, (b) U_1 transformation in QSAMb, (c) U_1 transformation in QSAMo, and (4) U_2 and U_3 transformation in both QSAMb and QSAMo. In these circuits, only the R_x rotation gates are used.

Table 1 Circuit complexity and the number of trainable parameters of QSAMb and QSAMo.

Model	Complexity*	Trainable parameters
QSAMb	48/88	19
QSAMo	32/72	18

* The number of qubits and two-qubit quantum gates

The two QSAM models are verified concretely in the numerical experiments using three public datasets, namely the Iris flower data, as well as the MC and RP datasets for text categorization. The numerical experiments were conducted using PennyLane [34].

In the following experiments, we use the binary cross-entropy loss,

$$L(\theta) = -\sum_{i=1}^N \left[y_{true} \log(\Pr[f(\langle M \rangle_{x,\theta})=1]) + (1-y_{true}) \log(\Pr[f(\langle M \rangle_{x,\theta})=0]) \right] \quad (11)$$

where $y_{true} \in \{0,1\}$ is the class label and $\Pr[f(\langle M \rangle_{x,\theta})=1]$ is the probability of the measurement outcome being 1. The Adam optimizer is utilized to update the parameters.

4.1. Iris classification

The first task involves the classification of Iris flowers into two categories [35]. The dataset consists of 100 data samples, with 50 samples per

category for setosa and versicolour Iris. Each sample contains four attributes: sepal length, sepal width, petal length, and petal width. During the learning process, 80 samples were allocated to the training set, and the remaining 20 samples were used as the test set.

The encoding circuit $U_e(x_i)$ is implemented using only one R_x rotation gate, as shown in Fig. 3(a). Therefore, according to the architectures shown in Fig. 2, the number of qubits n_1 equals to one. The U_1 circuits used in QSAMb and QSAMo are shown in Fig. 3(b) and 3(c), respectively, which utilize three and two qubits. In order to simplify the architecture of U_2 and U_3 circuits, two qubits of U_1 and U_2 circuits are utilized as the input to the following circuits (i.e. $n_2=2, n_3=2$). Since each Iris data sample contains four attributes, the number of qubits used by U_2 and U_3 circuits is eight. Fig. 3(d) presents the eight-qubits U_2 and U_3 circuits, which use the circuit-block

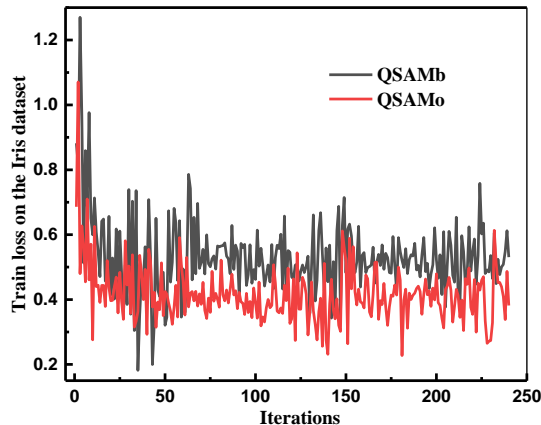


Fig. 4. Loss curves of the QSAMb and QSAMo models on the Iris dataset.

configuration of two-qubit gates [36]. For binary classification problems, only one qubit needs to be measured (i.e. $n_4=1$). The circuit complexity of QSAMb and QSAMo as well as their number of trainable parameters are shown in Table 1.

In the test using Iris dataset, both QSAMb and QSAMo models achieve a 100% classification accuracy, which indicates the two model’s ability to uncover the internal relationships between the four attributes of Iris flowers and their categories. Additionally, Fig. 4 shows that QSAMo has a faster convergence rate than QSAMb and exhibits smaller loss values. These results suggest that reducing redundant input data effectively reduces the complexity of the QSAM model, enhancing its overall effectiveness.

4.2. Text categorization

The second task involves binary text categorization using two public datasets, i.e. the MC and RP synthetic dataset [37]. MC contains 130 sentences and each sentence has three or four words. Half of the sentences are related to food and half to information technology (IT). The task of MC is to categorize a sentence as food or IT. There are totally 17 different words in MC and part of the vocabulary is in common between the two classes, so the task is not trivial. The learning process

utilizes 70 sentences for training, 30 for verification, and 30 for testing. On the other hand, RP contains 105 noun phrases containing relative clauses. There is an overall vocabulary of 115 words. The task of RP is also a binary-classification one, with the goal to predict whether a certain noun phrase contains a subject relative clause (“device that detects planets”) or an object relative clause (“device that observatory has”). The learning process utilizes 74 sentences for training and 31 for testing. In addition, the size of vocabulary and the sparseness of words make this task more challenging than the MC task.

For language datasets, the word is firstly represented by the word vector, which is typically obtained in the process of pre-trained word embedding. In this paper, we utilize the encoding circuit $U_e(x_i)$ to embed words, and compute the corresponding *Query*, *Key*, and *Value* vectors. Fig. 5 shows the circuits of encoding unit for MC and RP datasets. The encoding units use two qubits, so the number n_1 in Fig. 2 equals to two and U_1 circuits in QSAMb (QSAMo) utilize six (four) qubits. As it is in the Iris dataset, two qubits of U_1 and U_2 circuits are utilized as the input to the following circuits (i.e. $n_2=2$, $n_3=2$). Since each sentence sample contains four words, the number of qubits used by U_2 and U_3 circuits is eight. The U_1 , U_2 and U_3

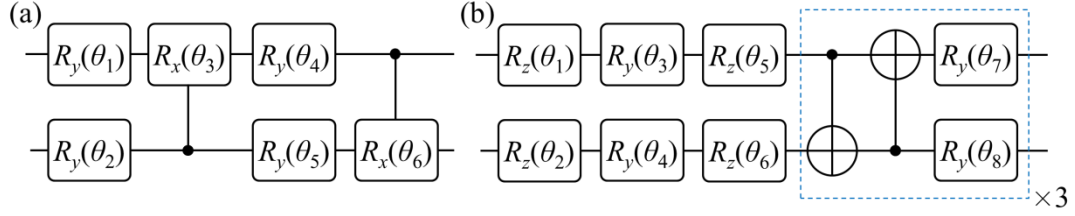


Fig. 5. Circuits of the encoder unit $U_e(x_i)$ for the dataset (a) MC and (b) RP. In MC, six parameters are used for word embedding, and in RP, 12 parameters are used.

Table 2 Circuit complexity and the number of trainable parameters of four quantum learning models as well as their classification accuracy for the MC and RP dataset.

Model	Complexity*		Trainable parameters		Accuracy (%)	
	MC	RP	MC	RP	MC	RP
DisCoCat[37]	—	—	40	168	79.80	72.30
QSANN[20]	24/24	48/240	25	109	100.00	67.74
QSAMb	96/136	96/136	22	22	100.00	72.58
QSAMo	64/104	64/104	20	20	100.00	74.19

* The number of qubits and two-qubit quantum gates

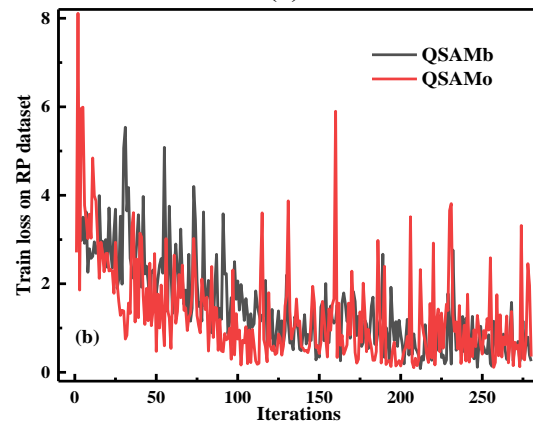
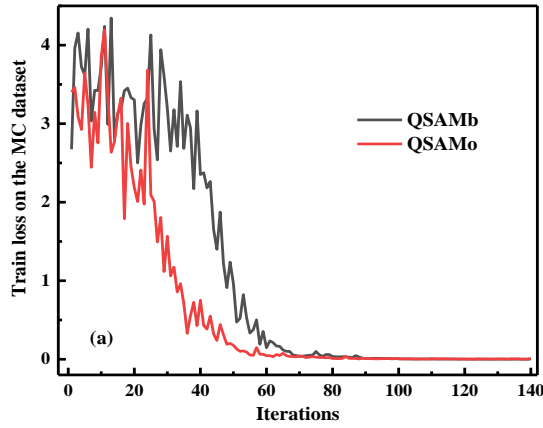


Fig. 6. Loss curves of the QSAMb and QSAMo models on the (a) MC and (b) RP dataset.

circuits are constructed using a circuit-block configuration of two-qubit gates as shown in Fig. 3(d). Finally, one qubit is measured to predict a label (i.e. $n_4=1$).

The circuit complexity of QSAMb and QSAMo as well as their number of trainable parameters are shown in Table 2. Note that the parameters in the encoder circuit are not counted in the total the number of trainable parameters as it is done in the QSANN mode [20], because the parameterized encoder could be replaced by pre-trained word embedding.

Table 2 shows that both the QSAMb and QSAMo models outperform other quantum learning models for NLP, such as DisCoCat [37] and QSANN [20]. In the MC task, both QSAMb and QSAMo achieve 100% classification accuracy; and in the RP task, QSAMb achieves 72.58% accuracy and QSAMo achieves 74.19% accuracy, both higher than the other two models. It's worth noting that the QSANN model is a quantum-classical hybrid model, where the PQC is used as a quantum-enhanced feedforward neural network to prepare *Query*, *Key*, and *Value* features, and other operations of SAM are implemented on the classical computer. Our QSAMs are complete quantum models. They achieve higher accuracy with significantly lower circuit complexity and fewer training parameters, demonstrating their powerful ability.

Additionally, Fig. 6 displays the training loss curves of the QSAMb and QSAMo models, which indicates that QSAMo has a faster convergence rate than QSAMb. This again suggest that reducing redundant input data can effectively enhance the model's effectiveness in text categorization task.

4.3. Robustness of QSAM

Finally, we demonstrate the robustness of our QSAM models against the quantum operation noises. For this experiment, we only use the QSAMo

model due to its superior performance in terms of complexity, convergence and accuracy. Three typical types of quantum noise are used, namely the bit-flip, depolarizing noise and amplitude-damping, which can be respectively described by the following Kraus operators,

$$K_0^b = \sqrt{1-p} \begin{pmatrix} 1 & 0 \\ 0 & 1 \end{pmatrix}, K_1^b = \sqrt{p} \begin{pmatrix} 0 & 1 \\ 1 & 0 \end{pmatrix}, \quad (12)$$

$$K_0^d = \sqrt{1-p} \begin{pmatrix} 1 & 0 \\ 0 & 1 \end{pmatrix}, K_1^d = \sqrt{p/3} \begin{pmatrix} 0 & 1 \\ 1 & 0 \end{pmatrix}, \quad (13)$$

$$K_2^d = \sqrt{p/3} \begin{pmatrix} 0 & -i \\ i & 0 \end{pmatrix}, K_3^d = \sqrt{p/3} \begin{pmatrix} 1 & 0 \\ 0 & -1 \end{pmatrix}$$

$$K_0^a = \begin{pmatrix} 1 & 0 \\ 0 & \sqrt{1-\gamma} \end{pmatrix}, K_1^a = \begin{pmatrix} 0 & \sqrt{\gamma} \\ 0 & 0 \end{pmatrix}. \quad (14)$$

Bit-flip is the most fundamental type of quantum noise, which has a certain probability p of flipping the state of a qubit (using the operator K_1^b), and a probability of $1-p$ of leaving the state unchanged (using the operator K_0^b).

Depolarizing noise is a more general form of quantum noise that compasses both bit-flip and phase-flip noise, providing a more comprehensive representation. Amplitude damping is used to model how interaction with the environment can impact the state populations of a qubit, with $\gamma \in [0, 1]$ representing the probability of amplitude damping.

We perform noise experiments by applying bit-flip, depolarization, and amplitude damping noise to the 0^{th} qubit of U_3 , which serves as the final measurement qubit. Table 3 shows the results, which reveal that the extent of noise's impact depends on the type of noise and the dataset being used. For a relatively simple learning task like Iris and MC, classification accuracy remains at 100% even when noise levels reach up to 0.1. However, for the RP task, a decrease in accuracy is observed as the

Table 3 Test accuracy of QSAMo on the Iris, MC and RP datasets using noisy quantum circuits.

Noise channel	Noise level p	Accuracy (%)		
		Iris	MC	RP
Zero noise	0	100	100	74.19
	0.001	100	100	74.19
	0.005	100	100	70.97
Bit-flip	0.01	100	100	58.06
	0.001	100	100	70.97
	0.005	100	100	64.51
Depolarizing	0.01	100	100	67.74
	0.001	100	100	64.52
	0.005	100	100	67.74
Amplitude Damping	0.01	100	100	61.29

noise level increases. Moreover, the bit-flip and amplitude damping noise have a greater impact than the depolarizing noise.

These findings suggest that our QSAM model is robust against quantum noise, so long as it possesses sufficient expressibility to learn the dataset. In other words, for a specific task, the critical factor still lies in finding an appropriate architecture for the QSAM network to learn the dataset and achieve high accuracy while also possessing strong resistance against quantum noise.

5. Conclusions

In this work, we propose a natural NISQ way of implementing SAM in QNNs by properly designing the method of data encoding and the architecture of PQC. Specifically, two architectures are developed, namely the QSAMb and QSAMo model. The data elements corresponding to different positions are encoded in group to calculate the attention scores and the attention vectors are approximated using the ansatz circuit. QSAMo is obtained by removing redundant information from QSAMb. We evaluated the performance of the two

QSAM models on several public datasets, including Iris classification and text categorization. QSAMo demonstrate a faster convergence rate than QSAMb and yield smaller loss values. In particular, our approach outperforms other quantum learning models in terms of accuracy and circuit complexity on the text categorization task. Moreover, we demonstrate the robustness of our model against quantum noise, such as the bit-flip, depolarizing, and amplitude-damping noise. The present work represents an important step of studying the quantum attention mechanism and the associated neural networks. The interesting future work includes (1) further optimizing the way of arranging the data encoding units to reduce the width complexity of the circuit; (2) optimizing the QSAM with better complexity and accuracy; (3) developing more complex quantum attention neural networks, such as the Transformer model, for various learning task based on the basic building blocks proposed in this work.

Acknowledgments

We are grateful to the support of

computational resources from the Marine Big Data Center of Institute for Advanced Ocean Study of Ocean University of China.

Funding

The present work was supported by the Natural Science Foundation of Shandong Province of China [grant numbers ZR2021ZD19] and the National Natural Science Foundation of China [grant numbers 12005212].

References

- [1] A. Vaswani, et al., Attention is all you need, NIPS. (2017), pp. 5998–6008. <https://doi.org/10.48550/arXiv.1706.03762>.
- [2] J. Devlin, M. W. Chang, K. Lee, K. Toutanova, Bert: Pre-training of deep bidirectional transformers for language understanding. (2018). <https://doi.org/10.48550/arXiv.1810.04805>.
- [3] A. Dosovitskiy, et al., An image is worth 16x16 words: Transformers for image recognition at scale. (2020). <https://doi.org/10.48550/arXiv.2010.11929>.
- [4] X. Wang, R. B. Girshick, A. Gupta, K. He, Non-local neural networks, Proceedings of the IEEE/CVF conference on computer vision and pattern recognition. (2018), pp. 7794–7803. <https://doi.org/10.1109/CVPR.2018.00813>.
- [5] Y. Li, et al., Efficient and Explicit Modelling of Image Hierarchies for Image Restoration. (2023). <https://doi.org/10.48550/arXiv.2303.00748>.
- [6] F. D. Keles, P. M. Wijewardena, C. Hegde, On the computational complexity of self-attention, in: International Conference on Algorithmic Learning Theory. (2023), pp. 597-619. <https://doi.org/10.48550/arXiv.2209.04881>.
- [7] F. Arute, et al., Quantum supremacy using a programmable superconducting processor, Nature. 574 (7779), (2019) 505-510. <https://doi.org/10.1038/s41586-019-1666-5>.
- [8] H. Zhong, et al., Quantum computational advantage using photons, Science. 370 (2020) 1460–1463. <https://doi.org/10.1126/science.abe8770>.
- [9] L. S. Madsen, et al., Quantum computational advantage with a programmable photonic processor, Nature. 606 (2022) 75–81. <https://doi.org/10.1038/s41586-022-04725-x>.
- [10] J. Preskill, Quantum computing in the NISQ era and beyond, Quantum. 79(2) (2018). <https://doi.org/10.22331/q-2018-08-06-79>.
- [11] K. Bharti, et al., Noisy intermediate-scale quantum algorithms, Reviews of Modern Physics. 94(1) (2022). <https://doi.org/10.1103/RevModPhys.94.015004>.
- [12] S. K. Jeswal, S. Chakraverty, Recent developments and applications in quantum neural network: a review, Archives of Computational Methods in Engineering. 26(4) (2019) 793-807. <https://doi.org/10.1007/s11831-018-9269-0>.
- [13] Y. Kwak, W. J. Yun, S. Jung, J. Kim, Quantum neural networks: Concepts, applications, and challenges, in: 2021 Twelfth International Conference on Ubiquitous and Future Networks (ICUFN). (2021) 413-416. <https://doi.org/10.1109/ICUFN49451.2021.9528698>.
- [14] M. Benedetti, E. Lloyd, S. Sack, M. Fiorentini, Parameterized quantum circuits as machine learning models, Quantum Science and Technology. 4(4) 043001 (2019). <https://doi.org/10.1088/2058-9565/ab4eb5>.
- [15] I. Cong, S. Choi, M. D. Lukin, Quantum convolutional neural networks, Nature Physics. 15(12) (2019) 1273-1278. <https://doi.org/10.1038/s41567-019-0648-8>.
- [16] J. Liu, K. H. Lim, K. L. Wood, W. Huang, C. Guo, H. L. Huang, Hybrid quantum-classical convolutional neural networks, Science China Physics, Mechanics Astronomy. 64(9) (2021) 1-8. <https://doi.org/10.1007/s11433-021-1734-3>.
- [17] J. Bausch, Recurrent quantum neural networks, Advances in neural information processing systems. 33 (2020) 1368-1379. <https://doi.org/10.48550/arXiv.2006.14619>.
- [18] Y. Li, et al., Quantum Recurrent Neural Networks for Sequential Learning. 2023. <https://doi.org/10.48550/arXiv.2302.03244>.
- [19] R. Zhao, J. Shi, S. Zhang, QSAN: A Near-term Achievable Quantum Self-Attention Network. 2022. <https://doi.org/10.48550/arXiv.2207.07563>.
- [20] G. Li, X. Zhao, X. Wang, Quantum self-attention neural networks for text classification. 2022. <https://doi.org/10.48550/arXiv.2205.05625>.

- [21] R. Di. Sipio, J. H. Huang, S. Y. C. Chen, S. Mangini, M. Worring, The Dawn of Quantum Natural Language Processing, in: ICASSP 2022 - 2022 IEEE International Conference on Acoustics, Speech and Signal Processing (ICASSP), Singapore, (2022), pp. 8612-8616. <https://doi.org/10.1109/ICASSP43922.2022.9747675>.
- [22] M. Cerezo, A. Arrasmith, R. Babbush, et al, Variational quantum algorithms, *Nat Rev Phys.* 3, (2021) 625–644. <https://doi.org/10.1038/s42254-021-00348-9>.
- [23] M. Schuld, N. Killoran, Quantum machine learning in feature Hilbert spaces, *Physical review letters.* 122(4) (2019). <https://doi.org/10.1103/PhysRevLett.122.040504>.
- [24] T. Hur, L. Kim, D. K. Park, Quantum convolutional neural network for classical data classification, *Quantum Machine Intelligence.* 4(1) (2022) 1-18. <https://doi.org/10.1007/s42484-021-00061-x>.
- [25] A. Kandala, et al., Hardware-efficient variational quantum eigensolver for small molecules and quantum magnets, *Nature.* 549(7671) (2017) 242-246. <https://doi.org/10.1038/nature23879>.
- [26] H. L. Tang, et al., Qubit - adaptive: An adaptive algorithm for constructing hardware-efficient ansatzes on a quantum processor, *PRX Quantum.* (2021) 020310. <https://doi.org/10.1103/PRXQuantum.2.020310>.
- [27] B. A. Martin, P. Simon, M. J. Rančić, Variational Hamiltonian Ansatz for 1D Hubbard chains in a broad range of parameter values. (2021). <https://doi.org/10.48550/arXiv.2111.11996>.
- [28] P. Busch, P. Lahti, J. P. Pellonpää, K. Ylinen, *Quantum measurement*, Berlin: Springer. (2016).
- [29] D. Wierichs, et al., General parameter-shift rules for quantum gradients, *Quantum.* 6 (2022): 677. <https://doi.org/10.22331/q-2022-03-30-677>.
- [30] A. Gilyén, S. Arunachalam, N. Wiebe, Optimizing quantum optimization algorithms via faster quantum gradient computation, in: *Proceedings of the Thirtieth Annual ACM-SIAM Symposium on Discrete Algorithms*, Society for Industrial and Applied Mathematics. (2019), pp. 1425-1444.
- [31] Z. Niu, G. Zhong, H. Yu, A review on the attention mechanism of deep learning, *Neurocomputing.* (2021) 48-62. <https://doi.org/10.1016/j.neucom.2021.03.091>.
- [32] H. Buhrman, et al., Quantum fingerprinting, *Physical Review Letters.* 87(16): 167902, (2001). <https://doi.org/10.1103/PhysRevLett.87.167902>.
- [33] D. Aharonov, V. Jones, Z. Landau, A polynomial quantum algorithm for approximating the Jones polynomial, *Proceedings of the thirty-eighth annual ACM symposium on Theory of computing.* (2006) 427-436. <https://doi.org/10.1145/1132516.1132579>.
- [34] B. Ville et al., PennyLane: Automatic differentiation of hybrid quantum-classical computations. 2018. <https://doi.org/10.48550/arXiv.1811.04968>
- [35] R.A. Fisher, (1936). <https://archive.ics.uci.edu/ml/datasets/iris>.
- [36] S. Sim, P. D. Johnson, A. Aspuru-Guzik, Expressibility and entangling capability of parameterized quantum circuits for hybrid quantum-classical algorithms, *Advanced Quantum Technologies.* 2 (12), 1900070, (2019). <http://doi.org/10.1002/qute.201900070>.
- [37] R. Lorenz, et al., QNLP in practice: Running compositional models of meaning on a quantum computer, *Journal of Artificial Intelligence Research.* 76 (2023) 1305-1342. <https://doi.org/10.1613/jair.1.14329>